PCCP

Accepted Manuscript

This is an *Accepted Manuscript*, which has been through the Royal Society of Chemistry peer review process and has been accepted for publication.

Accepted Manuscripts are published online shortly after acceptance, before technical editing, formatting and proof reading. Using this free service, authors can make their results available to the community, in citable form, before we publish the edited article. We will replace this *Accepted Manuscript* with the edited and formatted *Advance Article* as soon as it is available.

You can find more information about *Accepted Manuscripts* in the Information for Authors.

Please note that technical editing may introduce minor changes to the text and/or graphics, which may alter content. The journal's standard Terms & Conditions and the Ethical guidelines still apply. In no event shall the Royal Society of Chemistry be held responsible for any errors or omissions in this *Accepted Manuscript* or any consequences arising from the use of any information it contains.

ROYAL SOCIETY OF CHEMISTRY

www.rsc.org/pccp

PCCP

RSCPublishing

ARTICLE

Intrinsic magnetic properties of bimetallic nanoparticles elaborated by cluster beam deposition

Cite this: DOI: 10.1039/x0xx00000x

V. Dupuis,[a] G. Khadra,[a] A. Hillion,[b] A. Tamion,[a] J. Tuaillon-Combes,[a] L. Bardotti,[a] and F. Tournus.[a]

Received 00th January 2012,
Accepted 00th January 2012

DOI: 10.1039/x0xx00000x

www.rsc.org/

In this paper, we present some specific chemical and magnetic order obtained very recently on characteristic bimetallic nanoalloys prepared by mass-selected Low Energy Cluster Beam Deposition (LECBD). We study how the competition between d-atoms hybridization, complex structure, morphology and chemical affinity affects their intrinsic magnetic properties at the nanoscale. The structural and magnetic properties of these nanoalloys were investigated using various experimental techniques that include High Resolution Transmission Electron Microscopy (HRTEM), Superconducting Quantum Interference Device (SQUID) magnetometry, as well as synchrotron techniques such as Extended X-Ray Absorption Fine Structure (EXAFS) and X-Ray Magnetic Circular Dichroism (XMCD). Depending on the chemical nature of the nanoalloys we observe different magnetic responses compared to their bulk counterparts. In particular, we show how specific relaxation in nanoalloys impacts their magnetic anisotropy; and how finite size effects (size reduction) inversely enhance their magnetic moment.

A Introduction

Over the past few years, bimetallic magnetic nanoparticles (NPs) have attracted considerable attention as potential candidates for various applications from catalysis, magnetism, optics, to nanomedicine[1]. Nevertheless, experimental results on their magnetic properties are quite scarce because of intricate size and alloying effects. The atomic structure and magnetic behaviour of bimetallic NPs have been experimentally observed to differ from the corresponding bulk materials in a favourable way or not, due to small size effects as peculiar symmetry[2], partial chemical ordering[3], surface segregation[4]... Numerous theoretical works have been performed to try to explain exotic structure[5,6,7,8] or electronic properties[9,10] observed in such nanoalloys by integrating a great number of parameters.
In the one hand, as mentioned by Pierron-Bohnes et al.[11], both combined phenomena in nanoalloys can lead to enhancement of magnetic moment due to the cut bonds at the cluster surface and change in hybridization with other species orbitals. On the other hand, over all contributions (shape, strain and interface), the Magnetic Anisotropy Energy (MAE) is very sensitive to the spin-orbit coupling and to the chemical order but also to specific atomic relaxations in nanoalloys, which can give rise to oscillation for the first surface shells [12].

To illustrate chemical order effects on intrinsic magnetic properties of bimetallic NPs, we will present both experimental results and perspectives on ferromagnetic (FM) Fe or Co-based NPs with second element being 3d, 4d or 5d transition metal. Starting from promising bulk-phase diagrams for spintronic applications, a few miscible and immiscible couples will be reported. To give some ideas about the forthcoming developments, we will focus our attention on the magnetic moment and the MAE evolution with chemical order in well-defined nanoalloys. In order to work with ligand-free stoichiometric nanocrystals, the clusters were pre-formed in the gas phase thanks to a mixed equiatomic target and a laser vaporization source working in the Low Energy Clusters Beam Deposition (LECBD) regime. The apparatus equipped with a quadrupolar electrostatic mass-deviator allows depositing size-selected clusters in the 2-4 nm diameter range with sharp dispersion[13]. We previously showed that the shape of clusters prepared by LECBD followed the Wulff construction and that the anisotropic surface tension determines the shape of nanocrystal in equilibrium with the formation of facets[14]. Mass-selected clusters presented here, are co-deposited in an Ultra-High Vacuum (UHV) deposition chamber, with an independent atomic carbon matrix beam on 45°-tilted substrate[15]. To take interest in their intrinsic properties, NPs are 1%-diluted in volume to avoid magnetic interaction among NPs. As the inert carbon matrix offers an efficient external protection for sample transfer into air and a very good thermal resistance[16], subsequent vacuum high-temperature annealing is then possible to reach equilibrium phase without coalescence between NPs.
This paper, dealing with recent advanced results obtained on bimetallic nanoalloys prepared by LECBD, is divided versus NPs structure. The first part is dedicated to results on nanoalloys in tetragonal chemically ordered $L1_0$ phase (as in

Physical Chemistry Chemical Physics Accepted Manuscript

CoPt and FePt NPs), the second one on cubic B2 phase NPs (as in FeCo and FeRh NPs). Finally, the last part focuses on perspectives concerning in particular core/shell morphologies (as in FeAu, CoAu or CoAg NPs).

B Results and discussion

1) Chemically ordered tetragonal $L1_0$ nanomagnets

The bulk CoPt and FePt phase diagrams are very rich[17]. In particular, for equiatomic CoPt (or FePt) bulk alloys in the chemically ordered $L1_0$ phase, an extremely high magnetocrystalline anisotropy is expected from the stacking of pure Co (or Fe) and Pt atomic planes in the [001] direction.
We have shown that as-prepared mass-selected CoPt and FePt NPs prepared by LECBD are mainly FCC truncated octahedrons in a chemically disordered A1 phase and transit to the chemically ordered $L1_0$ phase upon 500°C-annealing in vacuum by conserving size and morphology (see Fig. 1.2 and 1.5)[18]. We have also put into evidence some Multi-$L1_0$ domains particles by transmission electron microscopy (TEM)[19].

The magnetic properties of CoPt (resp. FePt) clusters embedded in carbon matrix assemblies have been studied from Superconducting Quantum Interference Device (SQUID) magnetometry experiments and simulations. In order to measure the clusters magnetic intrinsic properties we have to check that the magnetic interactions are negligible in the samples. For this purpose we use Isothermal Remanent Magnetization (IRM) and Direct current Demagnetization (DcD) curves at 2 K[20]. Experimentally for the IRM, this consists in considering a sample initially demagnetized, initially at zero field, and apply a magnetic field before removing it to measure the remanent magnetization. For the DcD, the sample magnetization is, initially, the remanent magnetization. These new protocols are then used to detect the nature of interactions via the well know parameter δm=DcD(H)-(IRM(∞)-2IRM(H)). Without interaction, the δm parameter is equal to 0 whatever the applied magnetic field, whereas the presence of magnetizing or demagnetizing interactions leads respectively to $\delta m > 0$ and $\delta m < 0$. As presented in figure 1.3 the δm parameters is equal to 0 whatever the applied magnetic field, meaning that the magnetic interactions between the clusters are negligible in the sample.

Then we use the recently developed accurate "triple fit" method, where the Zero field Cooled/Field Cooled (ZFC/FC) susceptibility curves and a room temperature magnetization loop are entirely simultaneously fitted (see Fig. 1.4)[21]. For the CoPt samples, we have reached a reliable determination of the magnetic particle diameter (D_m) and the effective MAE normal distribution (characterized by the mean value K_{eff} and the standard deviation ω_K) which are reported in Table I [22].

	As prepared	Annealed
D_m (nm)	3.12 ± 0.1	3.12± 0.1
K_{eff}(kJ.m^{-3})	218 ± 20	293 ± 30
ω_K	37% ± 5%	28% ± 5%

Table I: Magnetic characteristics of as-prepared and annealed size-selected CoPt clusters embedded in carbon matrix with 3 nm in diameter.

In a previous paper[23,24] we have shown that the MAE in pure clusters essentially comes from the effect of additional facets and dispersion is relatively small. In the case of size-selected CoPt or FePt NPs assemblies, even with small shape and composition variations, a supplementary contribution to the MAE dispersion is to be considered due in particular to the statistical chemical distribution[25]. Indeed, since the anisotropy enhancement in as-prepared CoPt compared to pure Co clusters is due to the presence of Pt atoms, the dispersion of the magnetocrystalline anisotropy (which depends on the neighbourhood of each Co atom) increases with the number of possible chemical arrangements. It is probably the reason why the MAE of chemically disordered CoPt particles is quite large even if mass-selected clusters have small size dispersion (8% determined by TEM). Moreover, the main difference between the as-prepared and annealed samples comes from the magnetic anisotropy evolution. Upon annealing, as long as a well-defined and high enough degree of chemical order can be reached, the multiplicity of atomic configurations is strongly reduced and the effective MAE dispersion is expected to decrease while its median value increases[26]. Nevertheless, the effective MAE distribution of chemically ordered CoPt clusters only increase by 35 % for K_{eff} compared to the one of as-prepared sample (see Table I). This last value is one order of magnitude smaller than what is expected for the $L1_0$ bulk CoPt.

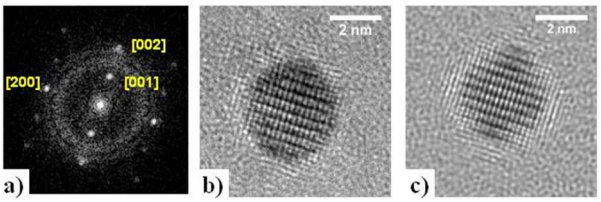

Fig. 1.2: a) Fourier transform of the experimental HRTEM image of a CoPt cluster where the chemical $L1_0$ order is visible. (b). The [001] peak is the signature of the chemical order in the nanoparticle. c) Simulated HRTEM image of a perfectly ordered cluster.

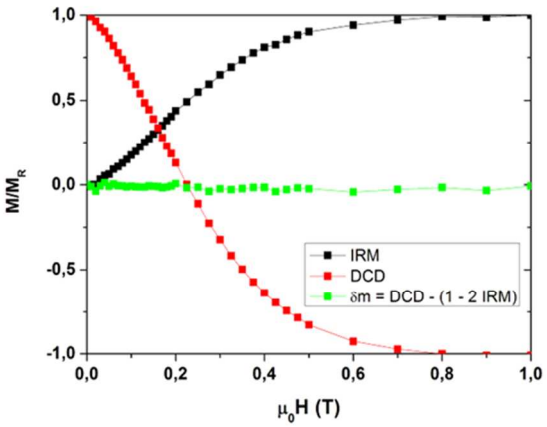

Fig. 1.3: IRM(H), DcD(H) *and* δm for annealed CoPt clusters embedded in an amorphous carbon matrix. The values presented here are divided by the remanent magnetization ($M_R = IRM(\infty)$).

Physical Chemistry Chemical Physics Accepted Manuscript

This journal is © The Royal Society of Chemistry 2012

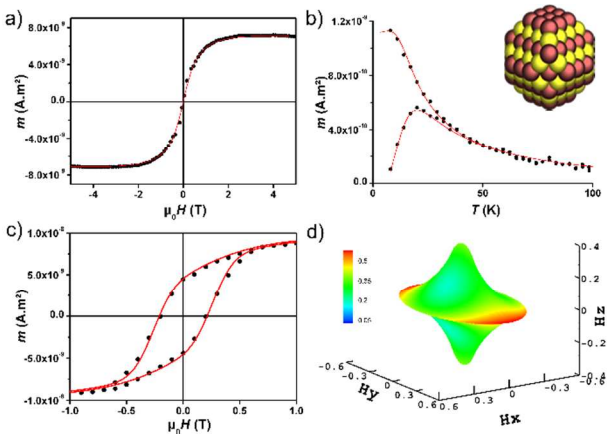

Fig. 1.4 Hysteresis loops at 300 K (a), at 2 K (c) and ZFC/FC (b) for annealed CoPt NPs embedded in C matrix. The solid lines correspond to the fit. Mean astroids associated to the biaxial fit (d).

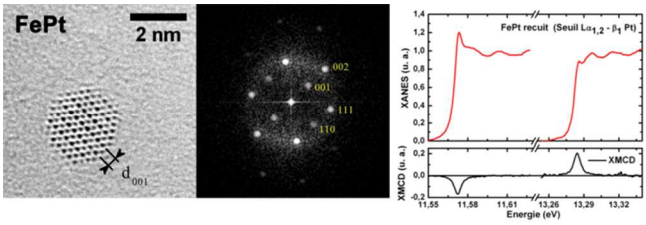

Fig. 1.5: Experimental HRTEM image and corresponding Fourier transform obtained on a FePt cluster where the chemical $L1_0$ order is visible (left). Evidence of induced magnetic moment in Pt from XMCD measurement at $L_{2,3}$ Pt edge (right).

To go further, the hysteresis loops at 2 K have been fitted using a geometrical approach[27,28,29]. At the cluster surface, the cubic symmetry is broken which involves second-order dominating terms. Briefly, the anisotropy function of a macro-spin can be expressed as:

$$\boldsymbol{G(\theta,\varphi) = K_1 m_z^2 + K_2 m_y^2}\,,$$

with z the easy axis, y the hard axis, x the intermediate axis and $K_1<0<K_2$. Here K_1 and K_2 represent the second order anisotropy constants, m_z the normalized magnetization projection on the easy axis. Finally θ and φ represent the magnetization angles in a spherical basis. In a case of a biaxial anisotropy we use the geometric approach to build the astroid which represents, in the field space, the magnetic switching field (H_{sw}). To take into account the thermal fluctuations (here at 2 K), which can bring the magnetization over the energy barrier, we use the Néel's relaxation model[30]. When two stable positions exist the relaxation time between these states is given by: $\boldsymbol{\tau = \tau_0 \exp(\Delta E/k_B T)}$, where τ_0 is a constant close to 10^{-10} s and ΔE the energy barrier. It is therefore possible to simulate hysteresis loops of an assembly of NPs taking into account the temperature, the size distribution and clusters' biaxial anisotropy (figure 1.4). We obtained bi-axial K_1 and K_2 terms with a constant ratio (K_2/K_1) close to 0.5[31].
In any case, such second order surface anisotropy terms are far away from the volume magnetocrystalline value expected for the $L1_0$ bulk-structure. Because MAE strongly depends on the local atomic distortions, we performed on French CRG BM02 and BM30B beam lines at the ESRF, X-ray diffraction and absorption at each metallic edge in view to reach quantitative lattice parameters in the 3d and 5d neighboring. We obtained nontrivial structural relaxations on size-selected CoPt and FePt clusters assembly in the 2-4 nm diameter range[32]. Indeed, we have found element-specific dependences of the relaxed inter-reticular parameters in such bimetallic clusters. Even for a very good chemical $L1_0$ order at nanoscale, this translates into a strong distortion in pure magnetic Co and Fe planes, not matching with the Pt inter planes and a large dispersion in the local 3d-environment. In particular, by spin-polarized density-functional calculations using the Vienna ab initio simulation package (VASP), we have shown that in the uppermost [001] Co layer, the Co atoms show a clear in-plane tetramerization.[33] Such complex specific atomic rearrangements in nanoalloys provide the basis for a microscopic understanding of the electronic and magnetic properties and could explain previously reported anisotropy lowering.[34]

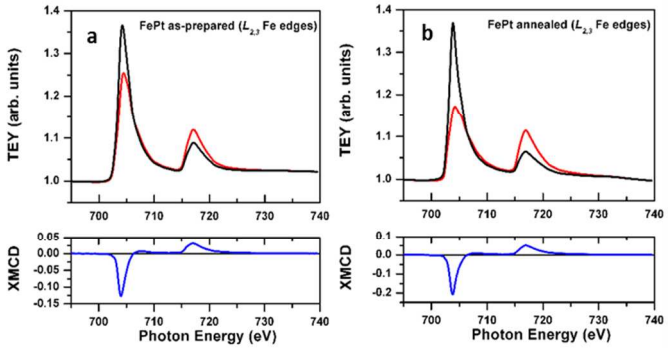

Fig.1.6: Comparison between the XMCD signal at the Fe-L edge obtained on as-prepared (a) and annealed (b) size selected FePt clusters embedded in carbon matrix with 3 nm in diameter.

In order to correlate the atomic magnetic moments to finite size effect in nanoalloys, we use XMCD spectroscopy experiments at each specific Co (resp. Fe) and Pt L-edges, on bimetallic CoPt (resp. FePt) nanoclusters around 3 nm in diameter (figure 1.5 and 1.6). Compared to the bulk, we find large magnetic moments of Fe, Co and Pt for the chemically ordered $L1_0$-like clusters. In Table II, the mean orbital and spin magnetic moments per Co, Fe and Pt atom, μ_L and μ_S have been determined using the well-known sum rules[35,36] and the number of holes per Co, Fe and Pt atoms estimated from theoretical band structure calculations for $L1_0$ CoPt and FePt (n_h Co $=$ $2.628, n_h$ Fe $=$ 3.705 and n_h Pt $=$ 2.369)[37]. We have found an enhancement of all the specific magnetic moments in FePt and CoPt clusters compared to the ones of the bulk phase. As the average spin moment is very sensitive to the cluster size[38], the enhanced proportion of low coordinated atoms at the surface (which corresponds to around 40 % in the 3nm size–range) causes a narrowing of the valence d band inversely proportional to the density of state at the Fermi level. This is probably the reason why for $L1_0$ 3 nm FePt and CoPt clusters, we have found spin moments that are always larger than the ones in the bulk chemically ordered phase. Concerning the orbital moment, in strongly hybridized systems with large SO coupling as in our case, a simple correlation to the MAE cannot be applied anymore[39]. The significant increase of μ_L/μ_S ratio has to be related to SO coupling and to the reduced symmetry at

Physical Chemistry Chemical Physics Accepted Manuscript

the surface which leads to a lower effective quenching of the μ_L moment in our diluted cluster assemblies compared to the bulk[40].

XMCD at various L3,2 edges	Co-edge	Fe-edge	Pt-edge
	μ_S (μ_B/at.)	μ_S (μ_B/at.)	μ_S (μ_B/at.)
	μ_L (μ_B/at.)	μ_L (μ_B/at.)	μ_L (μ_B/at.)
	μ_L/μ_S	μ_L/μ_S	μ_L/μ_S
CoPt as-prepared	**1.67**		**0.47**
	0.13		0.07
	0.077		0.15
CoPt annealed	**1.98**		**0.52**
	0.2		0.1
	0.101		0.192
FePt as-prepared		**1.33**	-
		0.15	
		0.11	
FePt annealed		**2.59**	**0.57**
		0.37	0.07
		0.14	0.13

TABLE II. Atomic spin μ_S, orbital μ_L magnetic moment and corresponding μ_L/μ_S ratio from XMCD at each specific Co (resp. Fe) and Pt $L_{2,3}$ edge on as-prepared and annealed CoPt and FePt cluster assemblies. The corresponding values for Fe and Co bulk can be found in the reference[41]. Note that the Pt moments of FePt particles have been measured on a sample with a broader size distribution (but equivalent median diameter).

As a conclusion, a careful examination of the intrinsic magnetic properties of well-defined chemically ordered $L1_0$-like CoPt and FePt nanoclusters has shown that finite size effects lead to opposite consequences on magnetic anisotropy and magnetic moments, respectively reduction and enhancement values compared to the bulk ones. This means that the stimulating results reported on literature for CoPt and FePt nanoalloys may have been over-interpreted because extrinsic effects, as magnetic interactions in highly concentrated cluster assemblies, matrix or coalescence effects upon annealing, have been neglected. Therefore, one can legitimately question their ability to keep its promises as high density storage media because their performance may never be high enough to ensure a magnetization thermal stability compatible with practical applications at room temperature.

From a fundamental point of view, these experimental results demonstrate the urgent need for theoretical non-colinear calculations-including the spin-orbit coupling, in order to obtain a quantitative evaluation of the effective MAE values in relaxed $L1_0$ nanoclusters.

2) Chemically ordered CsCl B2 nanomagnets

Near equiatomic composition of, both, FeRh and FeCo bulk alloys present CsCl-like B2 chemically ordered phase[42]. Moreover, a temperature-induced metamagnetic transition from anti-ferromagnetic to FM order (AFM→FM) is observed close to ambient for B2 FeRh alloy with great potential in spintronics and heat assisted magnetic recording [43,44,45]. Indeed, at room temperature, bulk B2 FeRh has been found to be a G-type AFM with a total magnetic moment on the iron atoms of 3.3 μ_B and no appreciable moment on the rhodium atoms. While above the 370 K transition temperature, the atomic moments of Fe and Rh are ferromagnetically aligned and take on total values of 3.2 and 0.9 μ_B, respectively [46,47,48]. It has long been known that the bcc unit cell volume expands by 1% upon transforming to FM order[49]. From first-principles and model theoretical investigations, the relative stability of the FM and AFM of α-bulk FeRh solutions have been shown to depend strongly on the interatomic distances[50] and recent experiments suggest that distortions of the bcc structure may also occur in bulk phase[51]. Such open condensed-matter questions enhance the appeal of small FeRh particles as specific example of 3d-4d nanoscale alloy with interatomic distances and unit cell distortions[52,53] inducing a strong modified magnetic phase diagram. As an illustration, ab-initio calculations predicted FM down to 0 K for 8-atoms relaxed B2-like FeRh clusters[54] while first experiments on chemically synthesized FeRh NPs failed to evidence low temperature stability of the FM order because of partial B2 ordering, elemental segregation, and coalescence upon annealing[55,56,57]. Moreover, temperature dependent Curie-like behaviour and induced spin moment in pure small Rh clusters have been revealed from XMCD measurements by Barthem et al.[58].

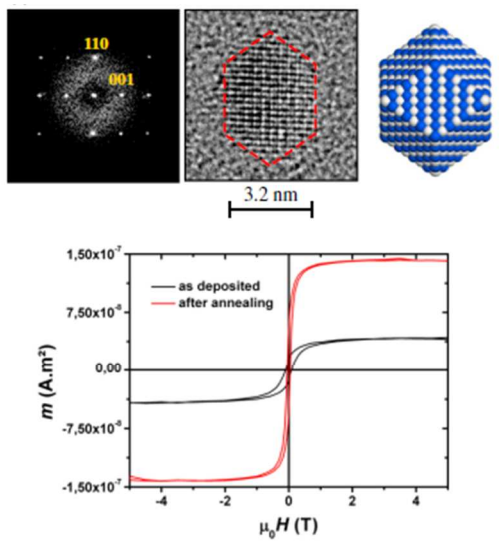

Fig. 2.1: Evidence of B2 phase from HRTEM observation obtained on annealed FeRh of 3 nm NPs (top). Hysteresis loops at 2 K obtained on 3 nm FeRh NPs showing the FM order and the global magnetization enhancement upon annealing (bottom)

Recently, we obtained the experimental persistence of high magnetization in FM order down to 2 K low-temperature for well-chemically ordered FeRh nanocrystals prepared by LECBD (see Fig.2.1)[59]. Once more, an annealing-driven

Physical Chemistry Chemical Physics Accepted Manuscript

This journal is © The Royal Society of Chemistry 2012

transition from a chemically disordered A1-like structure to a chemically ordered B2 structure with alternating atomic Fe and Rh layers and a bcc rhombic dodecahedron shape has been revealed from HRTEM on size-selected FeRh clusters with diameters up to 3 nm. Unlike SQUID and XMCD measurements have demonstrated ferromagnetic alignment of the Fe and Rh at low temperature with magnetic moments of 3 and 1μ_B, respectively. This ferromagnetic order has to be confronted to density-functional calculations.

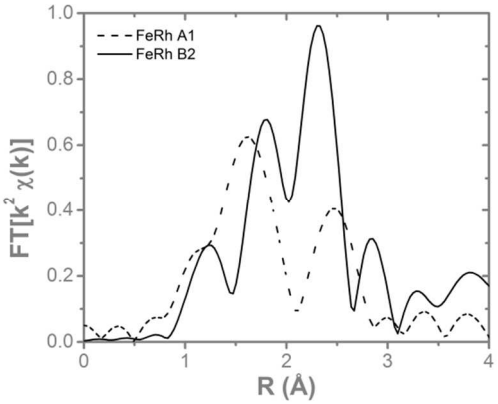

Fig. 2.2: Fourier Transform of the EXAFS signal in FeRh sample before (FeRh A1) and after annealing (FeRh B2).

A quantitative EXAFS analysis using the Artemis software[60], confirm the systematic transition upon annealing from the chemically disordered fcc A1 phase to the ordered bcc B2 one for 3nm-FeRh clusters assemblies embedded in carbon matrix. In particular a very good agreement has been obtained for the annealed sample with a bcc unit cell size (compatible with those of the B2 FeRh bulk) with a Debye Waller (DW) factor decreasing with chemical ordering[59]. Nevertheless the relatively large DW parameter probably due to different element relaxation (as already observed in CoPt nanoalloys), does not allow to obtain a perfect crystal at nanosize with specific magnetic order like compressed AFM and expanded FM as expected in the bulk phase. Moreover, one has to keep in mind that a FeRh nanoparticle with 3.3 nm in diameter count 35 % of atoms at the interface with metallic atoms on the inner shell and carbon matrix atoms in outer shell. This is in favour of FM order obtained at low temperature in FeRh nanoalloy because AFM state is probably incompatible with uncompensated spins at finite size.

As already mentioned, the challenge for ultimately using NPs as recording media, is to overcome the superparamagnetic limit at room temperature by using a material with huge magnetic anisotropy constant (K_{eff}). But in order to limit the required writing field (H_w), which is proportional to the ratio of K_{eff}/M_s, a large saturation magnetization (M_s) is also required. According to the slater-Pauling graph, FeCo has the largest recorded M_s (see figure 2.3.), but remains a soft magnetic material in the bulk bimetallic phase[61]. Concerning the binary bulk phase diagram, the FeCo system is characterized by an extensive solid solution range between fcc Fe and fcc Co and a wide bcc-Fe solid solution region which transforms via a second order reaction into the ordered CsCl type phase FeCo (see Fig. 2.4).

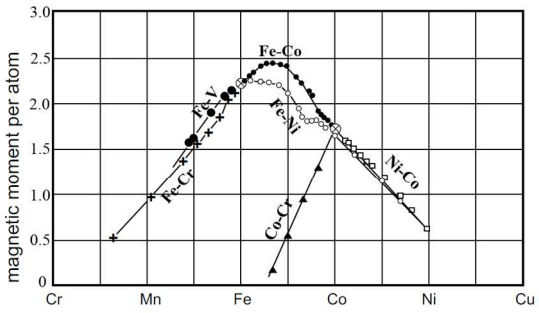

Fig. 2.3: Bulk Slater Pauling graph from ref [61]

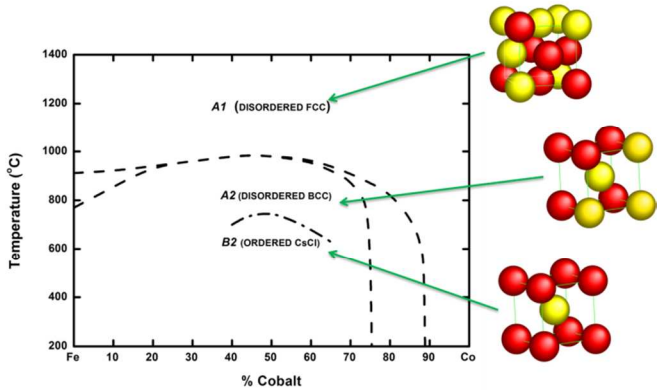

Fig. 2.4: Bulk FeCo Phase diagram adapted from ref [61]

Recent theoretical advances predicted that structural distortion in FeCo nanoalloys in chemically ordered B2 phases can lead to a giant MAE together with a large M_s (see Fig. 2.5)[62]. It is suggested that FeCo alloys grown in super lattice geometry on suitable buffers could be very promising with MAE comparable to that of chemically ordered FePt and it has never been experimentally confirmed. It is the reason why we have prepared FeCo NPs from LECBD, in view to try to increase the MAE by taking advantage of specific distortion expected in chemically ordered nano-alloys.

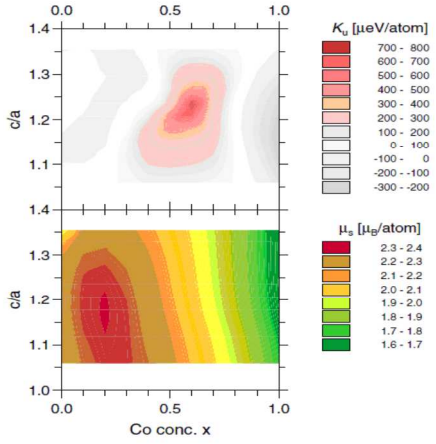

Fig. 2.5: (color). Calculated effective anisotropy K_u (upper panel) and saturation magnetic moment μ_s (lower panel) of tetragonal Fe_{1-x} Cox as a function of the c/a ratio and the Co concentration x, from ref [62].

Physical Chemistry Chemical Physics Accepted Manuscript

To reach this purpose, X-ray absorption spectroscopy (XAS) experiments at both Fe and Co K-edges, has been performed on FeCo NPs around 3 nm in diameter. On one hand, the crystallographic ordering has been promoted by high temperature annealing in vacuum without coalescence of such bimetallic clusters assemblies embedded in amorphous carbon matrix[63]. But as for HRTEM images, the low Z-contrast between Fe and Co atoms did not allowed for the moment to conclude without ambiguity between bcc and B2 chemically ordered phase upon annealing. Nevertheless SQUID magnetometry measurements were performed on our as-prepared and annealed samples. Simultaneous fitting of the ZFC-FC curves and the hysteresis $M(H)$ with the triple-fit protocol [21] shows an enhancement of the MAE after annealing almost doubles as seen Table III.

	As Prepared	Annealed (750 K)
T_{max} (K)	11	23
K_{eff} (kJ/m^3)	42 ± 2	110 ± 5
D_m (nm)	3.2 ± 0.1	3.3 ± 0.1
σ	0.32 ± 0.05	0.27 ± 0.05

Table III - Maximum of the ZFC susceptibility curves (T_{max}), magnetic anisotropy constant K_{eff}, and magnetic size parameters (median diameter D_m and standard deviation σ) as deduced from triple fit adjustments of SQUID measurements. For comparison, D_m and σ as determined from TEM observations are 3.1±0.1 nm and 0.32±0.05 nm, respectively.

In addition, X-ray magnetic circular dichroism (XMCD) measurements were performed on these samples at both Co and Fe $L_{2,3}$ edges on the DEIMOS beamline at SOLEIL (France). An increase of the magnetic moment per atom was observed at both Co and Fe edges in agreement with the chemical order.

C Perspectives

Besides the investigation of nanoalloy particles, where the two chemical species can mix together (with or without a chemical order) and present original features due to finite size effects, other geometries of bimetallic NPs are also appealing. This is the case of core-shell structures, or Janus-type particles where the two elements are immiscible. This is what is expected for NPs made of a magnetic transition metal (Fe or Co) and a noble metal (Ag or Au). Such mixed NPs offer additional possibilities for new functionalities (biocompatibility, detection, targeting, reactivity and catalysis...), and open the way to a very recent field of magneto-plasmonics with the aims of combining optical properties (localized surface plasmon resonance, LSPR) and magnetic properties[64,65,66]. While multilayers such as Fe/Au or Co/Au have been studied in the past (for magneto-optical or GMR effects...)[67,68,69], there are very few measurements on small bimetallic NPs. Moreover, as particles are mostly chemically-synthesized with large sizes or dispersions, there is almost no reported result on NPs in the size range between 2 and 5 nm in diameter. This is why the LECBD technique, with the deposition of mass selected clusters in a non-magnetic matrix, can bring new information on these interesting nano-systems.

Starting from the FeAu bulk phase diagram[70] as there is no compound at room temperature and a wide miscibility gap, competitions between core/shell NPs and nanoalloys (which may be obtained thanks to the out-of-equilibrium formation process) can be expected. At nanoscale, according to intrinsic thermodynamic considerations, gold atoms tend to segregate at FeAu NPs surface because of lower surface energy and larger atomic distance compared to iron. But in the other hand, equi-atomic, fcc FeAu alloys are quite easily stabilized at room temperature despite the fact that the fcc phase is only a high temperature bulk-phase[71]. New phases displaying a chemical order, such as the $L1_0$ phase for FeAu or the $L1_2$ phase for $FeAu_3$, can also be obtained at nanosizes while they are inexistent for the bulk material[72,73,74,75].

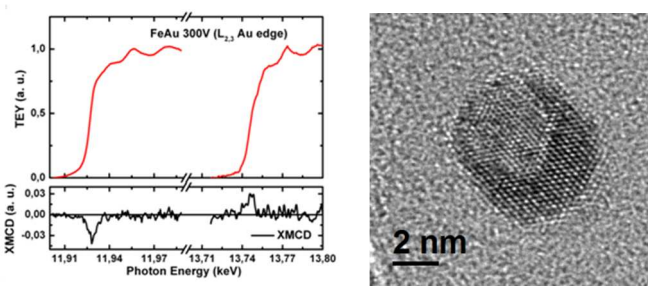

Figure 3.1: Evidence of induced magnetic moment on Au atoms from XMCD measurement at the $L_{2,3}$ Au edge (left) for as-prepared FeAu clusters (around 3 nm diameter) embedded in amorphous carbon. HRTEM image of an annealed CoAu nanoparticle (capped with carbon), displaying a core/shell structure with an off-centered Co core surrounded by an Au shell.

The magnetic polarization of a non-magnetic metal due to the proximity of a ferromagnetic metal is of great fundamental interest and can be studied by XMCD [76, 77]. For instance, we have been able to measure (at the ESRF ID12 beamline) the magnetic moment of gold atoms in 3 nm diameter FeAu clusters embedded in carbon (see Fig. 3.1): upon annealing, it evolves from 0.04 to 0.07μ_B/atom for the spin moment, while the orbital moment remains around 0.02 μ_B/atom. Even if the magnetic moment induced in Au from the hybridization with Fe is one order of magnitude lower than the one induced in Pt-based nanoalloys (FePt and CoPt), it remains sizeable and could play a role in magneto-plasmonic effects for instance. Note that in this size range, equiatomic core-shell structures are the most promising because the polarization of the noble metal is expected to be maximum with one monolayer of noble metal at the surface.

CoAu can also be produced by LECBD and promising results have already been obtained. In this system, where the two elements are immiscible, it is expected that gold will segregate at the surface. In agreement with theoretical calculations[78,79], a Co@Au core/shell structure is indeed observed after annealing (see Fig. 3.1). However, disordered alloys (which can be inhomogeneous) may exist for as-prepared particles that can be trapped in a metastable state. Such an alloy does not exist for the bulk and should therefore present original properties (magnetic and magneto-optic).

Physical Chemistry Chemical Physics Accepted Manuscript

This journal is © The Royal Society of Chemistry 2012

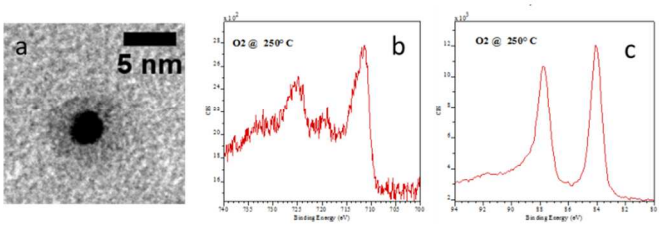

Fig. 3.2: TEM (a), XPS features of Fe-2p (b) and Au-4f (c) experiments performed on uncoated FeAu NPs annealed in oxygen at 250°C.

The impact of the particles' environment is critical in the case of core/shell particles: a reverse structure can be formed by changing the atmosphere or matrix leading for instance to $Au@Fe_xO_y$ or $Au@Co_xO_y$ NPs [80,81,82,83,84,85]. Namely, we have observed that the bare FeAu NPs (i.e. unprotected against exposition to air) display a $Au@Fe_2O_3$ core/shell morphology. For uncoated NPs, we have performed HRTEM and XPS observations where we clearly detect a pure metallic Au core and hematite (α-Fe_2O_3) shell morphology (see Figure 3.2). In this case, as the hematite phase is an AFM iron oxide, no magnetic signal is expected, contrary to ref [86]. The use of an oxide matrix, such as MgO, also has a drastic effect on the chemical arrangement, as compared to the more inert carbon matrix. In the case of FeAu NPs embedded in MgO matrix, we performed EXAFS experiments at both Fe K-edge and Au L-edge and found that more than the half of iron atoms is in contact with oxygen of the MgO matrix while the majority of gold are in homogeneous Au-Au environment. This preliminary result confirms that the segregation of iron atoms at the surface of nanoalloy is promoted in this case by their greater oxygen chemical affinity compared to the non-oxydizing gold atoms. This illustrates that the oxidation of the magnetic elements could be an extrinsic drawback for magneto-plasmonic application (the transparent dielectric matrix has to be chosen with care) but it also shows how playing with the NPs' environment can offer additional ways to tailor the structural and magnetic properties. Further investigations along this route will enable a better control of these complex nanosystems.

Conclusions

In summary, we have demonstrated that for small size alloyed NPs specific relaxations play an important role in governing and defining the structural and magnetic properties. We put in evidence the effects of finite size, alloying as well as chemical ordering on the intrinsic magnetic properties of CoPt and FeRh nanoalloys. In addition, active research on both nanoalloys (FeCo, FePt, etc...) as well as nanohybrids (CoAu, FeAu, etc...) is underway, with the advantage in terms of functionalization and consequently potential applications.

Acknowledgements

The authors are grateful to A. Ramos, H. Tolentino, M. de Santis and O. Proux for their help during EXAFS experiments on the French CRG-D2AM and BM30b-FAME beamlines at ESRF, to S. Rusponi and H. Brune from EPFL for stimulating discussions, J. Dreiser, C. Piamonteze and F. Nolting from Swiss Light Source for their investment on the X-Treme beamline, and A. Rogalev and F. Wilhelm for the XMCD measurements on the ESRF ID12 beamline. Support is acknowledged from both GDR CNRS 3182 and COST-STSM-MP0903 on Nanoalloys. All the clusters samples were prepared in the PLYRA [b] plateform thanks to the technical assistance of O. Boisron and C. Albin (ILM, Lyon) while SQUID measurements were performed at the CML [c] plateform.

Notes and references

[a] Institut Lumière Matière, UMR 5306, Université Lyon 1-CNRS, Université de Lyon, 69622 Villeurbanne cedex, France
[b] Plateform Lyonnaise de Rechecherche sur les Agrégats, Université Lyon 1-CNRS, Université de Lyon, 69622 Villeurbanne cedex, France
[c] Centre de Magnétomètrie de Lyon, Université Lyon 1-CNRS, Université de Lyon, 69622 Villeurbanne cedex, France

[1] Nanoalloys -- From Fundamentals to Emergent Applications, 2013, edited by Florent Calvo, published by Elsevier
[2] F. Tournus, K. Sato, T. J. Konno, T. Epicier, V. Dupuis, Phys. Rev. Letters 2013, **110**, 055501
[3] N. Jaouen, D. Babonneau, J. M. Tonnerre, D. Carbone, F. Wilhelm, A. Rogalev, T. K. Johal, and G. van der Laan, Phys. Rev. B 2007, **76**, 104421
[4] Antoniak, J. Lindner, M. Spasova, D. Sudfeld, M. Acet, M. Farle, K. Fauth, U. Wiedwald, H.-G. Boyen, P. Ziemann, F. Wilhelm, A. Rogalev, and S. Sun, Phys. Rev. Lett. 2006, **97**, 117201
[5] G. Rossi, R. Ferrando, and C. Mottet, Faraday Discuss. Chem. Soc. 2008, **138**, 193
[6] M. E. Gruner, G. Rollmann, P. Entel, and M. Farle, Phys. Rev. Lett. 2008, **100**, 087203
[7] P. Entel, M. E. Gruner, G. Rollmann, A. Hucht, S. Sahoo,, T. Zayak, H. C. Herper, and A. Dannenberg, Philos. Mag. 2008, **88**, 2725
[8] P. Andreazza, C. Mottet, C. Andreazza-Vignolle, J. Penuelas, H. C. N. Tolentino, M. De Santis, R. Felici, and N. Bouet, Phys. Rev. B 2010, **82**, 155453
[9] C. Barreteau and D. Spanjaard, J. Phys.: Condens. Matter 2012, **24** 406004
[10] R. Cuadrado and R. W. Chantrell, Phys. Rev. B 2012, **86,** 224415
[11] Nanoalloys: Synthesis, Structure and Properties. 2012, edited by D. Alloyeau, C. Mottet, C. Ricolleau, published by Springer. See "Magnetism of low-dimension Alloys" pp 287-330
[12] R. Guirado-Lopez, Phys. Rev. B, 2001, **63**, 174420.
[13] R. Alayan, L. Arnaud, A. Bourgey, M. Broyer, E. Cottancin, J.R. Huntzinger, J. Lermé, J.L. Vialle, M. Pellarin and G. Guiraud, Rev. Scient. Instrum. 2004, **75**, 2461

Physical Chemistry Chemical Physics Accepted Manuscript

[14] Perez A., Dupuis V., Tuaillon-Combes J., Bardotti L., Prevel B., Bernstein E., Melinon P., Favre L., Hannour A., Jamet M., Advanced Engineering Materials 2005, **7**, 475
[15] Tournus F., Blanc N., Tamion A., Hillenkamp M., Dupuis V., Journal of Magnetism and Magnetic Materials 2011, **323**, 1868
[16] N. Jaouen, D. Babonneau, J. M. Tonnerre, D. Carbone, F. Wilhelm, A. Rogalev, T. K. Johal, and G. van der Laan, Phys. Rev. B 2007, **76**, 104421
[17] Sanchez, J.M., Moran-Lopez, J.L., Leroux, C., Cadeville, M.C, J. Phys. C8, 1988, **49**, 107
[18] Blanc N., Tournus F., Dupuis V., Epicier T. Phys. Rev. B 2011, **83**, 092403
[19] Tournus F., Sato K., Epicier T., Konno T. J., Dupuis V. Phys. Rev. Lett. 2013, **110**, 055501
[20] A. Hillion, A. Tamion, F. Tournus, O. Gaier, E. Bonet, C. Albin, and V. Dupuis, Phys. Rev. B **88**, 094419
[21] Tamion A., Bonet E., Tournus F., Raufast C., Hillion A., Gaier O., Dupuis V., Phys. Rev. B 2012, **85**, 13443
[22] V. Dupuis, N. Blanc F. Tournus, A. Tamion, J. Tuaillon-Combes, L. Bardotti, O. Boisron, IEEE Trans. Magn. 2011, **47**, 3358.
[23] M. Jamet, W. Wernsdorfer, C. Thirion, D. Mailly, V. Dupuis, P. Mélinon, and A. Pérez, Phys. Rev. Lett. 2001, **86**, 4676
[24] Jamet M., Wernsdorfer W., Thirion C., Dupuis V., Melinon P., Perez A., Mailly D. Physical Review B, 2004 ,**69** , 024401
[25] F. Tournus, N. Blanc, A. Tamion, M. Hillenkamp and V. Dupuis, Phys. Rev. B 2010, **81**, 220405 (R)
[26] Tournus F., Rohart S., Dupuis V. IEEE Transactions On Magnetics, 2008, **44**, 3201
[27] A. Thiaville, J. Magn. Magn. Mater. 2004, **278**, 28
[28] A. Thiaville, Phys. Rev. B 2010, **61**, 12221
[29] A. Tamion, E. Bonet, F. Tournus, C. Raufast, A. Hillion, O. Gaier and V. Dupuis, Phys. Rev. B 2012, **85**, 134430
[30] L. Néel, Geophysique 1949, **5**, 99
[31] Dupuis V., Blanc N., Diaz-Sanchez L-E., Hillion A., Tamion A., Tournus F., Pastor G. M. , Eur. Phys. J. B, 2013, **86**, 1
[32] Dupuis V., Blanc N., Diaz-Sanchez L-E., Hillion A., Tamion A., Tournus F., Pastor G-M., Rogalev A., Wilhelm F., Eur. Phys. J. D 2013, **67**, 25
[33] Blanc N., Diaz-Sanchez L. E., Ramos A. Y., Tournus F., Tolentino H. C. N., De Santis M., Proux O., Tamion A., Tuaillon-Combes J., Bardotti L., Boisron O., Pastor G. M., Dupuis V. Phys. Rev. B 2013, **87**, 155412
[34] V. Dupuis and A. Tamion, Journal of Physics: Conference Series 2014, **521** 012001
[35] B. T. Thole, P. Carra, F. Sette, and G. van der Laan, Phys. Rev.Lett. 1992, **68**, 1943
[36] P. Carra, B. T. Thole, M. Altarelli, and X. Wang, Phys. Rev. Lett. 1993, **70**, 694
[37] I. Galanakis, M. Alouani and H. Dreysse: J. Magn. Magn. Mater. 2002, **242–245** 27
[38] Ohresser, P., Otero, E., Wilhelm, F., Rogalev, A., Goyhenex, C., Joly, L., Bulou, H., Romeo, M., Speisser, V., Arabski, J., Schull, G., & Scheurer, F., Journal of Applied Physics 2013, **114**, 223912.
[39] C. Andersson, B. Sanyal, O. Eriksson, L. Nordstr€om, O. Karis, D. Arvanitis, T. Konishi, E. Holub-Krappe, and J. Hunter Dunn, Phys. Rev. Lett. 2007, **99**, 177207
[40] K. W. Edmonds, C. Binns, S. H. Baker, S. C. Thornton, and C. Norris, J. B. Goedkoop, M. Finazzi, and N. B. Brookes, Phys. Rev. B 1999, **60**, 472
[41] C.T. Chen, Y.U. Idzerda, H.-J. Lin, N.V. Smith, G. Meigs, E. Chaban, G.H. Ho, E. Pellegrin, and F. Sette, Phys. Rev. Lett. 1995, **75**, 152
[42] O. Kubaschewski, Iron-binary phase diagrams, Springer-Verlag Berlin Heidelberg New York, 1982 (ISBN 3-11711-3).
[43] G. Shirane, C.W. Chen, P. A. Flinn, and R. Nathans, Phys. Rev. 1963, **131**, 183.
[44] J.-U. Thiele, S. Maat, and E. E. Fullerton, Appl. Phys. Lett. 2003, **82**, 2859.
[45] Z. Jia, N. Seetala, and R. Misra, Physica (Amsterdam) 2010, **405**, 2189
[46] M. Fallot, Ann. Phys. (N.Y.) 1938, **10**, 291
[47] E. Bertaut,A. Delapalme, F. Forrat, G. Roult, F. de Bergevin, and R. Pauthenet, J. Appl. Phys. 1962, **33**, 1123
[48] G. Shirane, C.W. Chen, P. A. Flinn, and R. Nathans, Phys. Rev. 1963, **131**, 183
[49] F. de Bergevin and L. Muldawer, C.R. Hebd. Seances Acad. Sci. 1961, **252**, 1347.
[50] M. E. Gruner, E. Hoffmann, and P. Entel, Phys. Rev. B 2003, **67**, 064415.
[51] T. Miyanaga, T. Itoga, T. Okazaki, and K. Nitta, J. Phys. Conf. Ser. 2009, **190**, 012097.
[52] F. Baletto and R. Ferrando, Rev. Mod. Phys. 2005, **77**, 371.
[53] R. Ferrando, J. Jellinek, and R. L. Johnston, Chem. Rev. 2008, **108**, 845.
[54] J. H. Mokkath and G. M. Pastor, Phys. Rev. B 2012, **85**, 054407.
[55] H.Y.Y. Ko and T. Suzuki, J. Appl. Phys. 2007, **101**, 09J103.
[56] D. Ciuculescu, C. Amiens, M. Respaud, A. Falqui, P. Lecante, R. E. Benfield, L. Jiang, K. Fauth, and B. Chaudret, Chem. Mater. 2007, **19**, 4624.
[57] Z. Jia, J.W. Harrell, and R. D. K. Misra, Appl. Phys. Lett. 2008, **93**, 22504.
[58] V. M. T. S. Barthem, A. Rogalev, F. Wilhel M. M. Sant'Anna, S. L. A. Mello, Y. Zhang, P. Bayle-Guillemaud, ,D. Givord, Phys. Rev. Lett. 2012, **109**, 197204
[59] Hillion A., Cavallin A., Vlaic S., Tamion A., Tournus F., Khadra G., Dreiser J., Piamonteze C., Nolting F., Rusponi S., Sato K., Konno T. J., Proux O., Dupuis V., Brune H. , Phys. Rev. Lett., 2013, **110**, 087207.
[60] B. Ravel and M. Newville, J. Synchrotron Radiat. 2005, **12**, 537.
[61] H. P. J.Wijn, ed.,Magnetic Properties of Metals: d-Elements, Alloys and Compounds (Springer, Berlin, 1991).
[62] Burkert T., Nordstorm L, Eriksson O. and Heinonen O., Phys. Rev. Lett. 2004, **93**, 027203.
[63] G. Khadra, A. Tamion, F. Tournus, B. Canut and V. Dupuis, special volume of Solid State Phenomena (Trans Tech Publications), in press 2015
[64] C. de Julian Fernandez, G. Mattei, E. Paz, R. L. Novak, L. Cavigli, L. Bogani, F. J. Palomares, P. Mazzoldi, A. Caneschi, Nanotechnology 2010, **21**, 165701
[65] F. Pineider, C. de Julian Fernandez, V. Videtta, E. Carlino, A. al Hourani, F. Wilhelm, A. Rogalev, P. Davide Cozzoli, P. Ghigna, C. Sangregorio, ACS Nano 2013, **7**, 857
[66] G. Armelles, A. Cebollada, A. García-Martín, M. U. González, Adv. Optical Mater. 2013, **1**, 10
[67] S. Honda, K. Koguma, M. Nawate, I. Sakamoto, J. Appl. Phys. 1997, **82,** 4428
[68] M. Mulloy, E. Velu, C. Dupas, M. Galtier, E. Kolb, D. Renard, J.P. Renard, J. Magn. Magn. Mater. 1995, **147**, 177.
[69] J. A. Barnard, M. R. Parker, D. Seale, J. Yang, IEEE Trans. Magn. 1993, **29**, 2711
[70] Binary Alloy Phase Diagrams, edited by T. B. Massalski ASM, International, Materials Park, OH, 1996
[71] Wilhelm, F.; Poulopoulos, P.; Kapaklis, V.; Kappler, J.-P.; Jaouen, N.; Rogalev, A.; Yaresko, A. N.; Politis, C. Physical Review B, 2008, **77**, 224414
[72] K. Sato, B. Bian, Y. Hirotsu, Jpn. J. Appl. Phys. 2002, **41**, L1

Physical Chemistry Chemical Physics Accepted Manuscript

 This journal is © The Royal Society of Chemistry 2012

[73] P. Mukherjee, P. Manchanda, P. Kumar, L. Zhou, M. J. Kramer, A. Kashyap, R. Skomski, D. Sellmyer, J. E. Shield, ACS Nano 2014, **8**, 8113
[74] P. Mukherjee, Y. Zhang, M. J. Kramer, L. H. Lewis, J. E. Shield, Appl. Phys. Lett. 2012, **100**, 211911
[75] Y. Vasquez, Z. Luo, R. E. Schaak, J. Am. Chem. Soc. 2008, **130**, 11866
[76] F. Pineider, C. de Julian Fernandez, V. Videtta, E. Carlino, A. al Hourani, F. Wilhelm, A. Rogalev, P. Davide Cozzoli, P. Ghigna, C. Sangregorio, ACS Nano 2013, **7**, 857
[77] C. de Julian Fernandez, G. Mattei, E. Paz, R. L. Novak, L. Cavigli, L. Bogani, F. J. Palomares, P. Mazzoldi, A. Caneschi, Nanotechnology 2010, **21**, 165701
[78] D. Bochicchio, R. Ferrando, Phys. Rev. B 2013, **87**, 165435
[79] A. Rapallo, J. A. Olmos-Asar, O. A. Oviedo, M. Ludueña, R. Ferrando, M. M. Mariscal, J. Phys. Chem. C 2012, **116**, 17210
[80] V. Papaefthimiou, F. Tournus, A. Hillion, G. Khadra, D. Teschner, A. Knop-Gericke, V. Dupuis, S. Zafeiratos, Chem. Mater. 2014, **26**, 1553
[81] B. Roldan Cuenya, L. K. Ono, J. R. Croy, A. Naitabdi, H. Heinrich, J. Zhao, E. E. Alp, W. Sturhahn, W. Keune, Appl. Phys. Lett. 2009, **95**, 143103
[82] T. Wen, K. M. Krishnan, J. Appl. Phys. 2011, **109**, 07B515
[83] Y.-H. Xu, J.-P. Wang, Adv. Mater. 2008, **20**, 994
[84] Y. Song, J. Ding, Y. Wang, J. Phys. Chem. C 2012, **116**, 11343
[85] J. Tuaillon-Combes, E. Bernstein, O. Boisron, P. Mélinon, Chem. Phys. Lett. 2013, **564**, 65
[86] F. Pineider, C. de Julián Fernández, V. Videtta, E. Carlino, A. al Hourani, F. Wilhelm, A. Rogalev, P.D. Cozzoli, P. Ghigna, C. Sangregorio, ACS Nano**,** 2013, **7**, 857

Physical Chemistry Chemical Physics Accepted Manuscript